This article was downloaded by: [Institute Of Atmospheric Physics]
On: 09 December 2014, At: 15:14
Publisher: Taylor & Francis
Informa Ltd Registered in England and Wales Registered Number: 1072954 Registered office: Mortimer House, 37-41 Mortimer Street, London W1T 3JH, UK

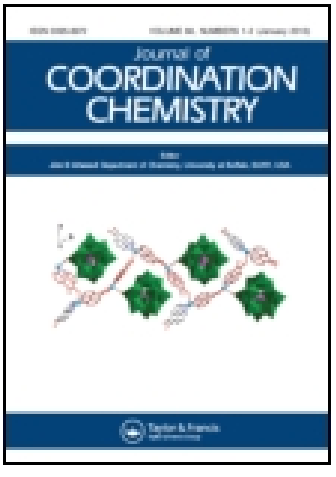

CrossMark
Click for updates

Journal of Coordination Chemistry
Publication details, including instructions for authors and subscription information:
http://www.tandfonline.com/loi/gcoo20

Synthesis, crystal structure description, electrochemical, and DNA-binding studies of "paddlewheel" copper(II) carboxylate

Muhammad Iqbal[a], Saqib Ali[a], Zia-Ur Rehman[a], Niaz Muhammad[b], Manzar Sohail[c] & Vedapriya Pandarinathan[d]

[a] Department of Chemistry, Quaid-i-Azam University, Islamabad, Pakistan

[b] Department of Chemistry, Abdul Wali Khan University, Mardan, Pakistan

[c] Faculty of Science, Health, Education and Engineering, University of the Sunshine Coast, Sippy Downs, Australia

[d] Faculty of Science & Engineering, Curtin University of Technology, Perth, Australia

Accepted author version posted online: 28 May 2014.Published online: 23 Jun 2014.

To cite this article: Muhammad Iqbal, Saqib Ali, Zia-Ur Rehman, Niaz Muhammad, Manzar Sohail & Vedapriya Pandarinathan (2014) Synthesis, crystal structure description, electrochemical, and DNA-binding studies of "paddlewheel" copper(II) carboxylate, Journal of Coordination Chemistry, 67:10, 1731-1745, DOI: 10.1080/00958972.2014.926337

To link to this article: http://dx.doi.org/10.1080/00958972.2014.926337

PLEASE SCROLL DOWN FOR ARTICLE

Taylor & Francis makes every effort to ensure the accuracy of all the information (the "Content") contained in the publications on our platform. However, Taylor & Francis, our agents, and our licensors make no representations or warranties whatsoever as to the accuracy, completeness, or suitability for any purpose of the Content. Any opinions and views expressed in this publication are the opinions and views of the authors, and are not the views of or endorsed by Taylor & Francis. The accuracy of the Content should not be relied upon and should be independently verified with primary sources of information. Taylor and Francis shall not be liable for any losses, actions, claims, proceedings, demands, costs, expenses, damages, and other liabilities whatsoever or

howsoever caused arising directly or indirectly in connection with, in relation to or arising out of the use of the Content.

This article may be used for research, teaching, and private study purposes. Any substantial or systematic reproduction, redistribution, reselling, loan, sub-licensing, systematic supply, or distribution in any form to anyone is expressly forbidden. Terms & Conditions of access and use can be found at http://www.tandfonline.com/page/terms-and-conditions

Downloaded by [Institute Of Atmospheric Physics] at 15:14 09 December 2014

Journal of Coordination Chemistry, 2014
Vol. 67, No. 10, 1731–1745, http://dx.doi.org/10.1080/00958972.2014.926337

Taylor & Francis
Taylor & Francis Group

Downloaded by [Institute Of Atmospheric Physics] at 15:14 09 December 2014

Synthesis, crystal structure description, electrochemical, and DNA-binding studies of "paddlewheel" copper(II) carboxylate

MUHAMMAD IQBAL†[1], SAQIB ALI*†, ZIA-UR REHMAN†, NIAZ MUHAMMAD‡, MANZAR SOHAIL§ and VEDAPRIYA PANDARINATHAN¶

†Department of Chemistry, Quaid-i-Azam University, Islamabad, Pakistan
‡Department of Chemistry, Abdul Wali Khan University, Mardan, Pakistan
§Faculty of Science, Health, Education and Engineering, University of the Sunshine Coast, Sippy Downs, Australia
¶Faculty of Science & Engineering, Curtin University of Technology, Perth, Australia

(*Received 16 December 2013; accepted 11 April 2014*)

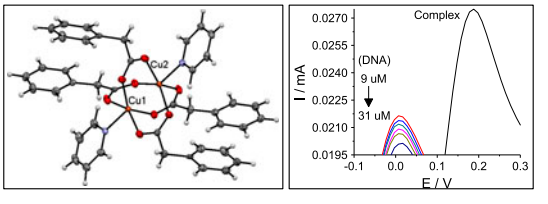

Dimeric paddlewheel copper(II) complex, pyCu(phenylacetate)$_4$Cupy, where py = pyridine, has been prepared and the crystal structure determined. Single crystal X-ray diffraction (XRD) revealed three crystallographically independent molecules in the unit cell. The geometry around each Cu(II) is square pyramidal with monodentate pyridine at the apical and bidentate carboxylates in the equatorial positions. The supramolecular structure of the complex arises primarily as a result of C–H···O along with some contribution of C–H···C interactions, resulting in the preferential alignment of the molecules along the *c*-axis. The purity of the crystalline complex has been confirmed through powder XRD study. Electrochemical solution study of the complex in aqueous DMSO (1 : 4) showed two redox couples corresponding to Cu(III)/Cu(II) and Cu(II)/Cu(I) irreversible electron transfer. The values of various voltammetric variables, such as diffusion coefficient (D_o), heterogeneous rate constant ($k°$), formal potential ($E°$), and charge transfer coefficient (α), have been calculated before and after DNA addition. DNA binding of the complex has been explored through cyclic voltammetry, UV–visible spectrophotometry, and viscosity measurement which have exhibited a mixed electrostatic and intercalative mode of interaction. Cyclic voltammetry indicated self-induced redox activation and potential anticancer ability of the complex, supported by UV–visible spectrophotometry as well as viscometry.

Keywords: Cu(II) complex; Crystal structure description; Detailed electrochemistry; UV–visible; DNA-binding study

1. Introduction

The inherent cumulative cytotoxic effects associated with platinum-based drugs have necessitated the search for new less toxic metal-based drugs [1–6]. Metal-based drugs exercise

*Corresponding author. Email: drsa54@yahoo.com
[1]Present address: Department of Chemistry, Bacha Khan University, Charsadda, Pakistan.

© 2014 Taylor & Francis

Downloaded by [Institute Of Atmospheric Physics] at 15:14 09 December 2014

superior qualities over organic-based drugs, owing to their variable structural properties and redox states, particularly in biologically accessible potential range. The latter property is especially important for biological applications of the drug under consideration [7–9].

The administration of a drug in an inactive form and its activation on reaching the target tissue of the biological systems is one of the most successful approaches used in the drug delivery systems. By applying this strategy, the deactivation of the drug while reaching its target tissue is minimized and a relatively high potency is expected. However, activation of the drug on reaching the target is a challenging issue. The trigger may be light, pH, or reducing cellular environment of the target tissue [7, 10, 11]. As the use of oxidizing agents for the activation of drug formed harmful byproducts, self-induced redox activation of the drug via exposing to the hypoxic environment of the target tissue is considered the most desirable for redox-active metal-based drugs [6, 7, 12–15].

The ability to undergo structural changes or electron transfer reactions under accessible biological potential drop arises from the structure of the drug molecule [16, 17]. Copper complexes have different reactivities and properties in different oxidation states [18, 19]; the moderate "hardness" of Cu(II) allows ligands to modify its redox ability and structural properties [20, 21].

The newly synthesized copper(II) complex has donors similar to those of *Casiopeinas* [22–24]. Here, the "syn" mode of coordination of carboxylate along with the N-donor accounts for the enhanced stability of Cu(II) species in the mixed aqueous solvent system, providing potent DNA binding of the complex in a low potential range despite the geometry restraints. The facile redox reactions of the complex under mild conditions herald its potential as a potent self-activatable cytotoxic drug. The DNA-binding activity of the synthesized complex is typical of structurally similar paddlewheel complexes that have been already reported [25–28]. The DNA-binding ability has been verified by UV–visible spectrophotometry and viscosity measurements.

2. Experimental

2.1. *Materials and methods*

Anhydrous $CuSO_4$, phenyl acetic acid, pyridine, $NaHCO_3$, KCl, and salmon sperm DNA (SSDNA) were obtained from Fluka, Switzerland. DMSO, methanol, and chloroform were obtained from Merck, Germany and used without drying and purification. Water used was singly distilled. The melting point was obtained in a capillary tube using a Gallenkamp, serial number C040281, UK, an electrothermal melting point apparatus. Powder X-ray diffraction (XRD) analysis was performed at 298 K on a PANalytical, X'Pert PRO diffractometer using Cu-Kα radiation ($\lambda = 1.540598$ Å). FT-IR spectra were recorded on a Nicolet-6700 FT-IR spectrophotometer, Thermoscientific, USA, from 4000 to 400 cm^{-1}.

2.2. *X-ray crystallographic studies*

Diffraction data were collected at 100(2) K on a beamline MX1 at the Australian Synchrotron ($\lambda = 0.708457$ Å) [29]. Data reduction and indexing of diffraction pattern were performed using XDS software [30]. The crystal structure was solved by direct methods, followed by refinement against F^2 with full-matrix least-squares method using SHELXL-97 [31]. All nonhydrogen atoms were refined with anisotropic displacement parameters.

Downloaded by [Institute Of Atmospheric Physics] at 15:14 09 December 2014

2.3. *Electrochemistry*

Voltammetric experiments were performed using an SP-300 potentiostat, serial number 0134, BioLogic Scientific Instruments, France. Measurements were carried out in an aqueous DMSO (1 : 4) solution containing 0.01 M KCl, under an N_2-saturated environment in a conventional three-electrode cell with a saturated silver/silver chloride electrode (Ag/AgCl) as reference, a thin platinum wire as a counter, and a bare glassy carbon electrode (GCE) with a surface area of 0.196 cm^2 as the working electrode. Prior to the experiment, the GCE was polished with alumina (Al_2O_3) on a nylon buffing pad followed by washing with acetone and finally with distilled water. Electrochemical measurements were carried out at room temperature (25 ± 0.5 °C).

2.4. *DNA interaction study by cyclic voltammetry*

An appropriate amount of SSDNA was dissolved in distilled water and stirred overnight. The nucleotide to protein (*N*/*P*) ratios of ~1.9 was obtained from the ratio of absorbance at 260 and 280 nm ($A_{260}/A_{280} = 1.9$), indicating that the SSDNA is sufficiently free from protein [32]. The SSDNA concentration was determined via absorption spectroscopy using the molar absorption coefficient of 6600 M^{-1} cm^{-1} (260 nm) for SSDNA [33]. Voltammograms of 1 mM solution of the complex, prepared in aqueous DMSO (1 : 4), were taken in the presence of 9, 10, 11, 14, 25, and 31 μM DNA.

2.5. *DNA interaction by absorption spectroscopy*

Solutions of the compound for UV–visible spectrophotometric analysis were prepared in aqueous DMSO (1 : 4) at 4 mM. The absorption titrations were performed by keeping the concentration of the compound fixed, while varying the SSDNA concentration. Equivalent solutions of SSDNA were added to the complex and reference solutions to eliminate the absorbance of SSDNA itself. Complex SSDNA solutions were allowed to incubate for 30 min at room temperature before measurements were made. Absorption spectra were recorded using cuvettes of 1 cm path length at room temperature (25 ± 1 °C).

2.6. *Viscosity measurements*

Solutions of the complex were prepared in aqueous DMSO (1 : 4). Viscosity measurements were carried out using a Ubbelohde viscometer at 25 ± 1 °C. Flow time was measured with a digital stopwatch. Each sample was measured three times and an average flow time was calculated. Data are presented as relative viscosity $(\eta/\eta_o)^{1/3}$, *versus* binding ratio ([complex]/[SSDNA]), where η is the viscosity of SSDNA in the presence of complex and η_o is the viscosity of DNA alone. Viscosity values were calculated from the observed flow time of SSDNA-containing solution (t_o), $\eta = t - t_o$ [34].

2.7. *General procedure for the synthesis of complex*

Sodium bicarbonate (0.504 g, 6 mM) was treated with an equimolar quantity of phenyl acetic acid (0.817 g, 6 mM) in distilled water at 60 °C. After neutralization of the acid with

base, an aqueous solution of copper sulfate (0.478 g, 3 mM) was added dropwise. The reaction mixture was stirred for 3 h at 60 °C and then methanolic solution of pyridine (0.24 mL, 3 mM) was added with constant stirring. Stirring was continued for another 3 h under the same reaction conditions.

The final product was filtered, washed thoroughly with distilled water, and air dried. The solid was recrystallized from a mixture of chloroform and methanol (1 : 1) and characterized using FT-IR and X-ray single crystal analysis.

Light blue crystals; m.p. 185 °C; yield (80%). λ_{max} (nm) = 723, ε (L M^{-1} cm^{-1}) = 130. FT-IR (cm^{-1}): 1624 ν(OCO)$_{asym}$, 1446 ν(OCO)$_{sym}$, $\Delta\nu$ = 178, 2915 νCH$_2$, 3032 ν(Ar–H), 1497 νAr(C=C), 1599 ν(C=N), 415 ν(Cu–O).

3. Results and discussion

3.1. *FT-IR data*

FT-IR spectra of the dimeric Cu(II) complex were in accord with the results of the X-ray single crystal analysis, having all the characteristic bands for its structure. The asymmetric and symmetric COO stretching vibrations of carboxylate showed bands at 1624 and 1446 cm^{-1}, respectively. The attachment of carboxylate to Cu(II) ion through oxygen was further supported by the appearance of the absorption band at 415 cm^{-1}, corresponding to Cu–O. The value of $\Delta\nu$ = $\{\nu_{asym}(OCO) - \nu_{sym}(OCO)\}$ calculated for the complex was 178 cm^{-1}, indicating a bridging bidentate coordination for carboxylate in the complex [35, 36]. The shift towards lower frequencies of C=N stretching bands, which were observed at 1599 cm^{-1} instead of their normally observed 1625–1610 cm^{-1} [37, 38], indicated the involvement of nitrogen of pyridine in coordination with Cu(II) [39]. This was further supported by the appearance of the pyridyl ring vibration band at 753 cm^{-1} [40]. The aromatic C=C and C–H stretches were observed at 1497 and 3032 cm^{-1}, respectively. Methylene C–H stretch was observed at 2915 cm^{-1}, supported by the presence of bands at 695 and 1398 cm^{-1} that correspond to its rocking and bending deformations, respectively.

3.2. *Powder XRD study*

Powder XRD of the synthesized complex was compared with the respective simulated spectrum by superimposing the spectra. The simulated and experimental powder XRD patterns are in complete agreement with each other for the complex as in figure 1, showing that the complex has been synthesized and crystallized in the pure form.

3.3. *Single crystal X-ray analysis*

Crystal structure of the complex is given along with the numbering scheme in figure 2, for which the main crystallographic parameters and details of the X-ray diffraction experiment are listed in table 1. The selected bond lengths and angles are listed in table 2. The complex crystallizes in triclinic system and contains three crystallographically independent molecules in the unit cell as shown in figure 3(A). Each molecule in the unit cell is a dimer having four carboxylates binding two copper ions in a bridging bidentate fashion, resulting in a

Downloaded by [Institute Of Atmospheric Physics] at 15:14 09 December 2014

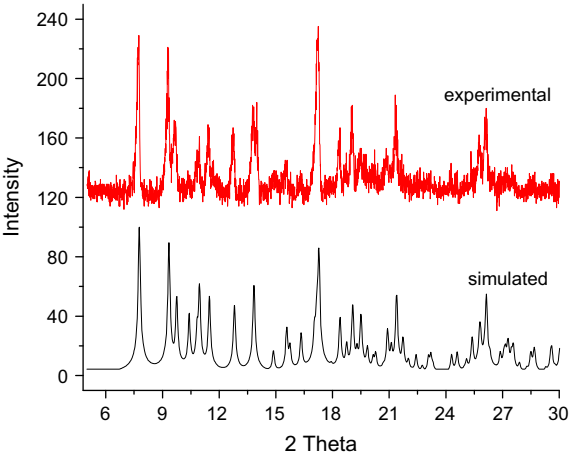

Figure 1. Experimental and simulated spectra of the complex.

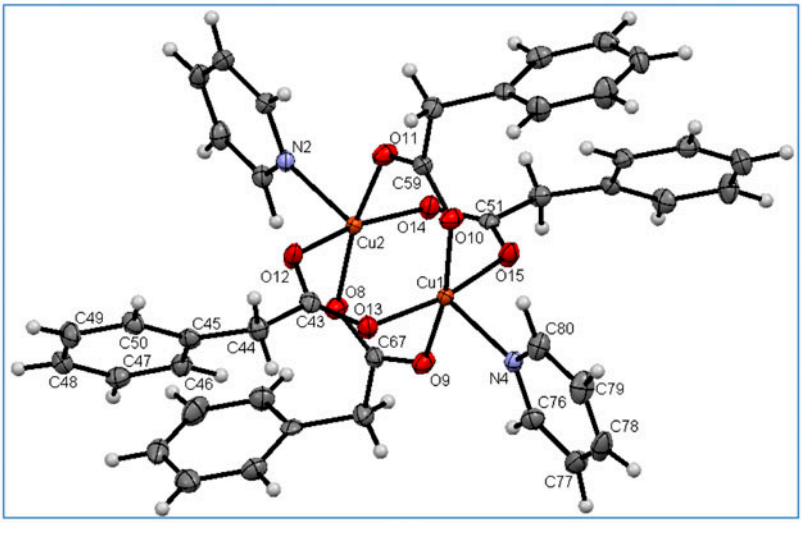

Figure 2. ORTEP drawing with the numbering scheme of the complex having formula $C_{42}H_{38}Cu_2N_2O_8$.

paddlewheel structure. The apical position is occupied by pyridine, resulting in a distorted square-pyramidal coordination geometry for each Cu(II). The Cu–Cu (2.6451(5)), Cu–O (average) (1.9757(2)), and Cu–N (2.1530(2) Å) distances are comparable to those observed for the structurally similar dimers of Cu(II) with trimethylacetate and substituted pyridine ligands, $[((2\text{-}NH_2)(6\text{-}CH_3)C_5H_3N)_2Cu_2(\mu\text{-}OOCCMe_3)_4]$ [41] and $[((NH_2)_2C_5H_3N)_2Cu_2(\mu\text{-}OOCCMe_3)_4{\cdot}C_6H_6]$ [42], where Cu–Cu = 2.730(1) and 2.762(1), Cu–O(average) = 1.963(2)–1.974(2) and 1.922(6)–2.019(5), and Cu–N = 2.296(3) and 2.243(3) Å, respectively. The small difference between the structural parameters of the synthesized complex and the cited

Downloaded by [Institute Of Atmospheric Physics] at 15:14 09 December 2014

Downloaded by [Institute Of Atmospheric Physics] at 15:14 09 December 2014

Table 1. Structure refinement parameters of the complex.

Empirical formula	$C_{42}H_{38}Cu_2N_2O_8$
Formula weight (g M^{-1})	825.86
Temperature (K)	100(2)
Wavelength (Å)	0.71073
Crystal system	Triclinic
Space group	$P\bar{1}$
a (Å)	11.0320(15)
b (Å)	16.619(2)
c (Å)	20.340(2)
α (°)	92.747(2)
β (°)	89.982(6)
γ (°)	93.035(3)
Volume (Å^3)	3719.6(8)
Z	4
Density (Calcd) (g cm^{-3})	1.475
Absorption coefficient (mm^{-1})	1.201
F (0 0 0)	1704
Crystal size (mm)	0.27 × 0.22 × 0.19
θ (°)	1.23–25
Index ranges	$-13 \le h \le 13$
	$-19 \le k \le 18$
	$-21 \le l \le 24$
Reflections collected	12,186
Independent reflections	9437
Data/restraints/parameters	9437/7/1278
Goodness-of-fit on F^2	1.087
Final R indices	$R_1 = 0.0383$
$[I > 2\sigma(I)]$	$wR_2 = 0.0944$
R indices (all data)	$R_1 = 0.0537$
	$wR_2 = 0.1009$

complexes arises partly from the variation in base strength of the N donor, which affects the Cu–N and Cu–O bond lengths [43]. The coordination environment around each copper of the complex is a $\{CuNO_4\}$ square pyramid, same as other paddlewheel complexes reported [44–47].

3.3.1. Supramolecular structure. Owing to the absence of sufficiently polar hydrogen, there is no H-bonding in the intermolecular interactions of the complex. However, the carboxylate oxygens of one molecule are close enough to establish C–H···O interactions with hydrogens at position-3 of the phenyl ring of the neighboring molecules lying on two opposite sides, resulting in an intermolecular arrangement preferentially along the *c*-axis as shown in figures 3(B) and 4(A). Such an interaction is impossible along the *b*- or *a*-axis, accounting for the sparse distribution of molecules along these two axes [see figure 4(B) and (C)]. The different arrangements of the molecules along the three axes may be due to the presence of three independent molecules in the unit cell. Comparing the supramolecular structure with those of Cu(II) complexes of *para*-substituted phenyl acetate derivatives of similar metal core [48], despite the higher number of intermolecular interactions in the synthesized complex, the molecules are not evenly distributed along the three axes and the packing is not as compact as those of the cited complexes [48]. This is also supported by the smaller density and larger crystal size of the synthesized complex compared to those of

Table 2. Selected bond lengths and angles of the complex.

Bond	Distances, Å
Cu(2)–O(1)	1.971(2)
Cu(2)–O(8)	1.975(2)
Cu(2)–O(14)	1.976(2)
Cu(2)–O(11)	1.981(2)
Cu(2)–N(2)	2.153(2)
Cu(1)–Cu(2)	2.6451(5)
Cu(1)–O(15)	1.968(2)
Cu(2)–O(14)	1.976(2)
Cu(1)–O(13)	1.970(2)
Cu(1)–N(4)	2.159(2)
	Angles, °
O(12)–Cu(2)–O(14)	167.37(8)
O(8)–Cu(2)–O(14)	88.68(9)
O(12)–Cu(2)–O(11)	88.72(9)
O(8)–Cu(2)–O(11)	167.98(8)
O(14)–Cu(2)–O(11)	90.46(9)
O(12)–Cu(2)–N(2)	97.63(9)
O(8)–Cu(2)–N(2)	98.53(9)
O(14)–Cu(2)–N(2)	94.99(9)
O(11)–Cu(2)–N(2)	93.49(9)
O(12)–Cu(2)–Cu(1)	85.43(6)
O(8)–Cu(2)–Cu(1)	85.06(6)
O(14)–Cu(2)–Cu(1)	81.96(6)
O(11)–Cu(2)–Cu(1)	82.95(6)
N(2)–Cu(2)–Cu(1)	175.28(6)
O(15)–Cu(1)–O(13)	167.70(8)
O(15)–Cu(1)–O(10)	90.51(9)
O(13)–Cu(1)–O(10)	88.65(9)
O(15)–Cu(1)–O(9)	89.06(9)
O(13)–Cu(1)–O(9)	89.11(9)
O (10)–Cu(1)–O(9)	167.47(8)
O(15)–Cu (1)–N(4)	98.50(9)
O(13)–Cu(1)–N(4)	93.77(9)
O(10)–Cu(1)–N(4)	98.26(8)
O(9)–Cu(1)–N(4)	94.19(8)
O(15)–Cu(1)–Cu(2)	85.39(6)
O(13)–Cu(1)–Cu(2)	82.31(6)
O(10)–Cu(1)–Cu(2)	84.72(6
O(9)–Cu(1)–Cu(2)	82.77(6)
N(4)–Cu(1)–Cu(2)	175.05(6)
O(12)–Cu(2)–O(8)	89.50(9)

Downloaded by [Institute Of Atmospheric Physics] at 15:14 09 December 2014

the cited complexes [48] (see table 1). The difference in the electrochemical behavior of the synthesized complex (where the reduction of Cu(II) has been shifted to more negative potential) with respect to the cited pair of the complexes may be attributed to the relatively higher stability of the Cu(II) species in case of the former, in the solvent system used in the experiment. This cannot be explained on the basis of the para-substituent effect on phenyl ring that is lying quite far from the electroactive metal center.

Downloaded by [Institute Of Atmospheric Physics] at 15:14 09 December 2014

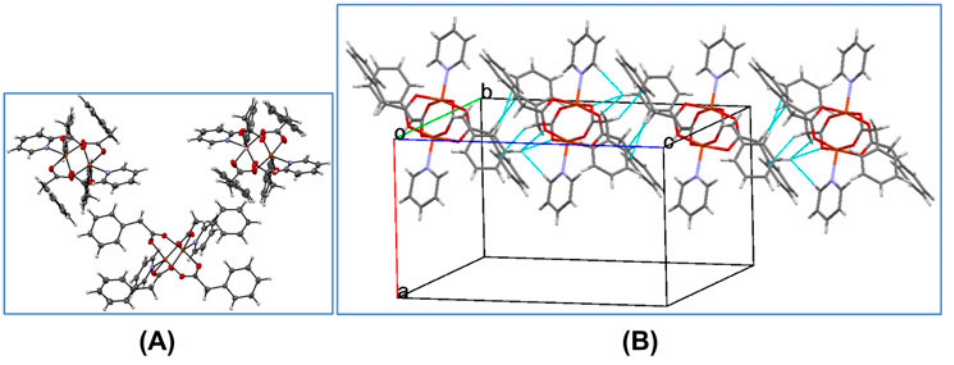

Figure 3. (A) Structure of the complex showing crystallographically independent molecules in its unit cell; (B) C–H···O and C–H···C interactions of the molecule (shown blue) (see http://dx.doi.org/10.1080/00958972.2014.926337 for color version).

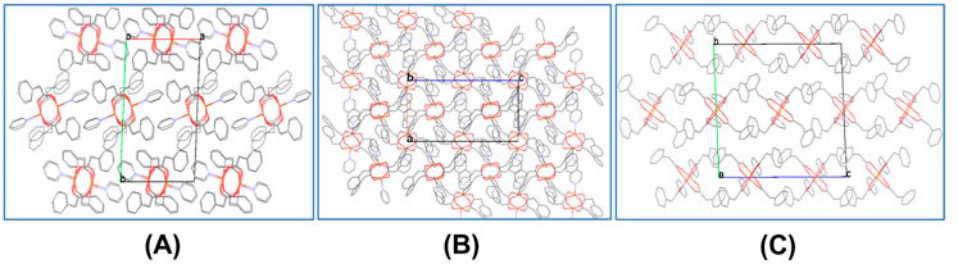

Figure 4. Relative arrangement of the molecules along different axes: (A) arrangement of molecules as viewed along the *c*-axis; (B) 3-D packing of the molecules viewed along the *b*-axis; (C) 3-D view of the molecules as viewed along the *a*-axis.

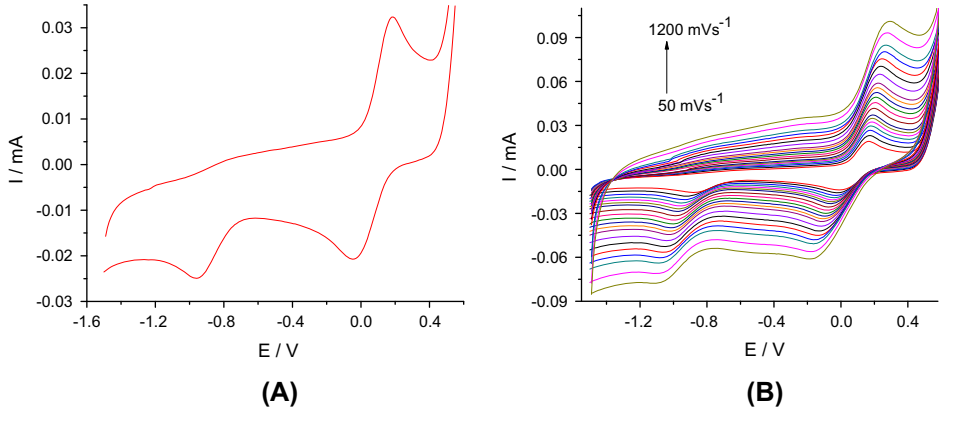

Figure 5. Cyclic voltammograms of 1 mM complex at a scan rate of 100 (A) and 50, 75, 100, 125, 150, 175, 200, 250, 300, 350, 400, 450, 500, 550, 600, 700, 800, 900, 1000, and 1200 mV s^{-1} (B).

Downloaded by [Institute Of Atmospheric Physics] at 15:14 09 December 2014

3.4. *Electrochemical studies*

Cyclic voltammetry was used to explore the electrochemical behavior of the complex, giving voltammograms at a scan rate of 100 mV s^{-1} and at different scan rates in figure 5(A) and (B), respectively. Two redox couples corresponding to Cu(III)/Cu(II) and Cu(II)/Cu(I) processes with $E_{p1/2}$ values of 0.105 and −0.812 V were observed, respectively. The redox pattern corresponding to the first redox couple of the complex is typical of other structurally related complexes [49–51]. The shifting of the second redox couple to a more negative potential is attributed to the stability of Cu(II) under the experimental conditions [52, 53] and has been found typical of other structurally related complexes [51, 54, 55]. The peak separation ($\Delta E_p = E_{pa} - E_{pc}$) values corresponding to Cu(III)/Cu(II) and Cu(II)/Cu(I) couples of the complex are 249 and 329 mV, respectively. On the basis of peak separation and other criteria of reversibility (i.e. i_{pa}/i_{pc} ratio and change of peak position with scan rate), the complex exhibits irreversible electron transfer [48, 56].

The nature of the redox processes was judged from the linearity of log i_p *versus* log v plots shown in figure 6(A) and (B), with slope values of 0.295 and 0.411 for oxidation and reduction processes, respectively. From the slope values, predominantly diffusion-controlled processes are indicated for the complex on the surface of the GCE [57].

The diffusion coefficient values for the redox processes were calculated using the Randles–Sevcik equation [58] (equation (1)),

$$i_p = (2.99 \times 10^5) n(\alpha n)^{1/2} A C^* D_o^{1/2} v^{1/2} \quad (1)$$

where i_p, α, n, D_o, C^*, A, and v denote the peak current in ampere, charge transfer coefficient, the number of electrons involved in the electron transfer process, diffusion coefficient in $cm^2 s^{-1}$, bulk concentration of the complex in M cm^{-3}, surface area of the working electrode in cm^2, and potential scan rate in V s^{-1}, respectively.

The slope values for D_o calculation were obtained using the respective i_p *versus* $v^{1/2}$ plots, shown in figure 7(A) and (B), for oxidation and reduction, respectively, and αn was calculated using the Bard and Faulkner relation [59] (equation (2)),

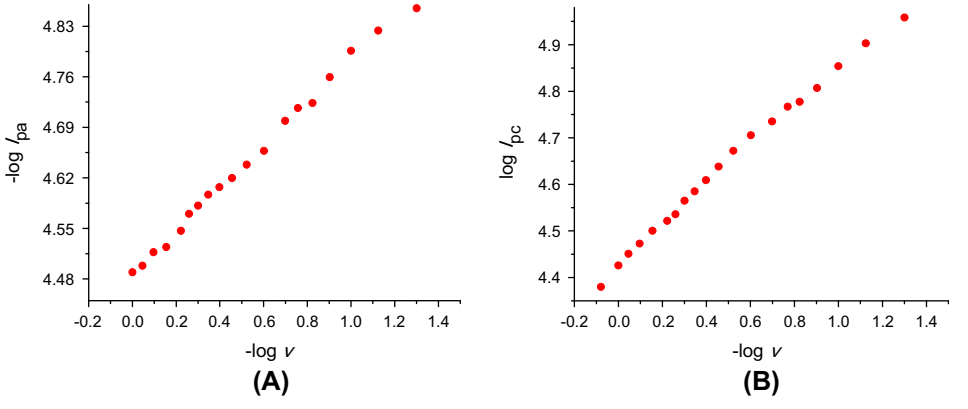

Figure 6. Plots of −log of anodic peak current (A) and log of cathodic peak current (B) *vs.* −log of scan rate for the complex.

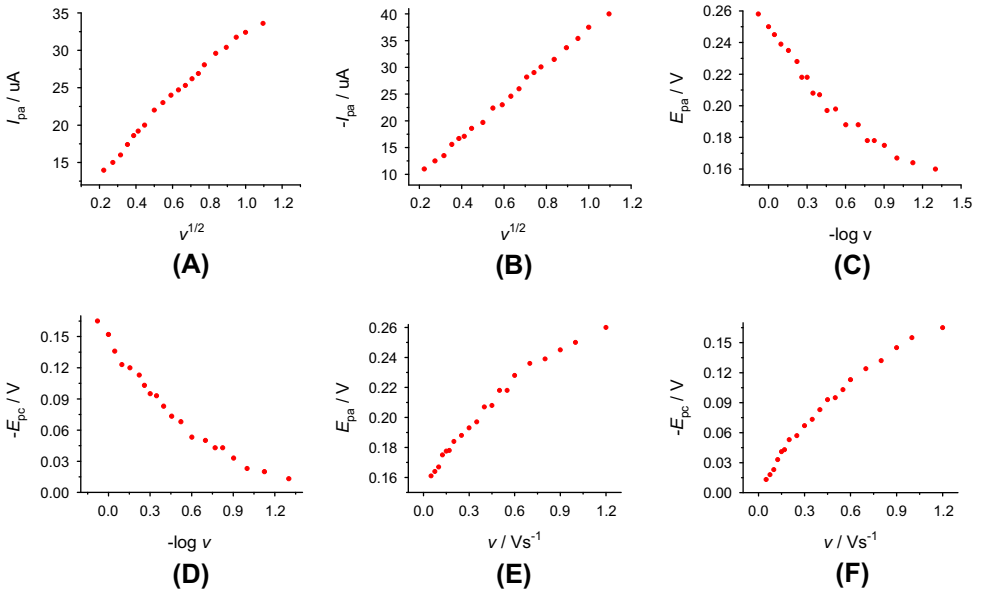

Figure 7. Plots of anodic and cathodic peak currents *vs.* square root of the scan rate (A), (B), anodic and cathodic peak potentials *vs.* −log of scan rate (C), (D), and scan rate (E) and (F) for the complex, respectively.

Table 3. Thermodynamic and kinetic parameters for the oxidation of the first redox couple of the complex obtained from cyclic voltammetry.

Complex	$E°$ (V)	αn	$D_o \times 10^6$ (cm^2s^{-1})	$k°$ (s^{-1})
Complex	0.160	0.561	0.73 ± 0.1	1.95
Complex-DNA	0.004	0.542	0.53 ± 0.1	1.01

Table 4. Thermodynamic and kinetic parameters for the reduction of the first redox couple of the complex obtained from cyclic voltammetry.

Complex	$-E°$ (V)	αn	$D_o \times 10^6$ (cm^2s^{-1})	$k°$ (s^{-1})
Complex	0.012	0.341	1.27 ± 0.1	0.03
Complex-DNA	0.130	0.397	1.09 ± 0.1	1.00

$$\alpha n = 47.7/[E_p - E_p/2]\text{mV} \quad (2)$$

where E_p is the peak potential and $E_p/2$ is the peak potential at half of the maximum peak current value.

The values of αn and $D_{o,}$ thus calculated are given in tables 3 and 4 for oxidation and reduction processes, respectively. D_o values are higher than those observed for the structurally similar and relatively higher molecular mass Cu(II) complexes of 4-chloro- and

Downloaded by [Institute Of Atmospheric Physics] at 15:14 09 December 2014

4-methoxy phenylacetate [48], confirming the inverse relationship between the molecular mass and the diffusion rate of the electroactive species towards the electrode surface.

The value of redox potential, E, is given by equation (3) [60–62]:

$$E = E^{\circ} + 2.303\,\mathrm{RT}k^{\circ}/\alpha nF - 2.303\,\mathrm{RT}/\alpha nF\ \log v \tag{3}$$

where $E°$ is the formal redox potential, $k°$ is the standard heterogeneous rate constant, and F is the Faraday constant. The values of heterogeneous rate constant ($k°$) were determined from the intercept of peak potential *versus* negative logarithm of scan rate plots [shown in figure 7(C) and (D)] by putting various oxidation and reduction parameters alternatively in equation (3). The values of formal potential ($E°$) were determined from the intercept of redox peak potential *versus* scan rate curve [figure 7(E) and (F)] by extrapolating the curve to the potential axis at $v = 0$.

$E°$ values thus calculated were 0.16 and –0.012 V for oxidation and reduction processes, respectively, as listed in tables 3 and 4. The values of $k°$, as calculated using equation (3), are presented in tables 3 and 4 for oxidation and reduction processes, respectively.

3.5. *DNA-binding study through cyclic voltammetry*

Cyclic voltammetry was employed to explore the DNA-binding ability of the complex at various scan rates, shown in figure 8(A). A shift of 0.17 V in potential to a less positive region (or to a more negative region in case of reduction signal) was observed on the addition of DNA as shown in figure 8(B), exhibiting electrostatic interaction with the complex [63]. However, after successive additions of SSDNA, there was an observable shift to the right-hand side indicating a concomitant intercalative mode of interaction with SSDNA as well [figure 8(C)]. In addition to the peak shift, the peak current decreased by about 7 μA in the presence of 14 μM DNA added to the 1 mM complex solution. The decrease in peak current and shift in potential are far more than those observed for other dimeric Cu(II) and Ni(II) complexes [49], indicating more efficient and facile interaction of the complex with DNA. The slope value of i_p *versus* $v^{1/2}$ plot [figure 8(D)] is reduced by the addition of DNA, indicating the binding of DNA with the complex [52, 64].

Cyclic voltammetric parameters have been determined and listed in tables 3 and 4, by repeating the cycles at different scan rates in the presence of 25 μM DNA [figure 8(A)]. The plots used for the calculation of D_o, E, $E°$, $k°$, and αn are shown in figure 8(D)–(I). The lower value of diffusion coefficient of DNA-bound complex ($5.3 \times 10^{-7}\,\mathrm{cm^2 s^{-1}}$) compared to that of the unbound complex ($7.3 \times 10^{-7}\,\mathrm{cm^2 s^{-1}}$) shows a reduction in the mobility of the former [65]. The heterogeneous rate constant also suffers a diminution in line with other changes as a result of interaction of the complex with SSDNA. The binding constant was determined from the intercept of the plot of log 1/[DNA] *versus* log $i_p/(i_o - i_p)$ [figure 8(J)] using equation (4) [66],

$$\log\left(1/[\mathrm{DNA}]\right) = \log K + \log i_p/(i_o - i_p) \tag{4}$$

where K is the binding constant, i_o and i_p are the peak currents of the complex in the absence and presence of DNA, respectively. The value of K calculated was $3.074 \times 10^3\,\mathrm{M^{-1}}$.

Downloaded by [Institute Of Atmospheric Physics] at 15:14 09 December 2014

Downloaded by [Institute Of Atmospheric Physics] at 15:14 09 December 2014

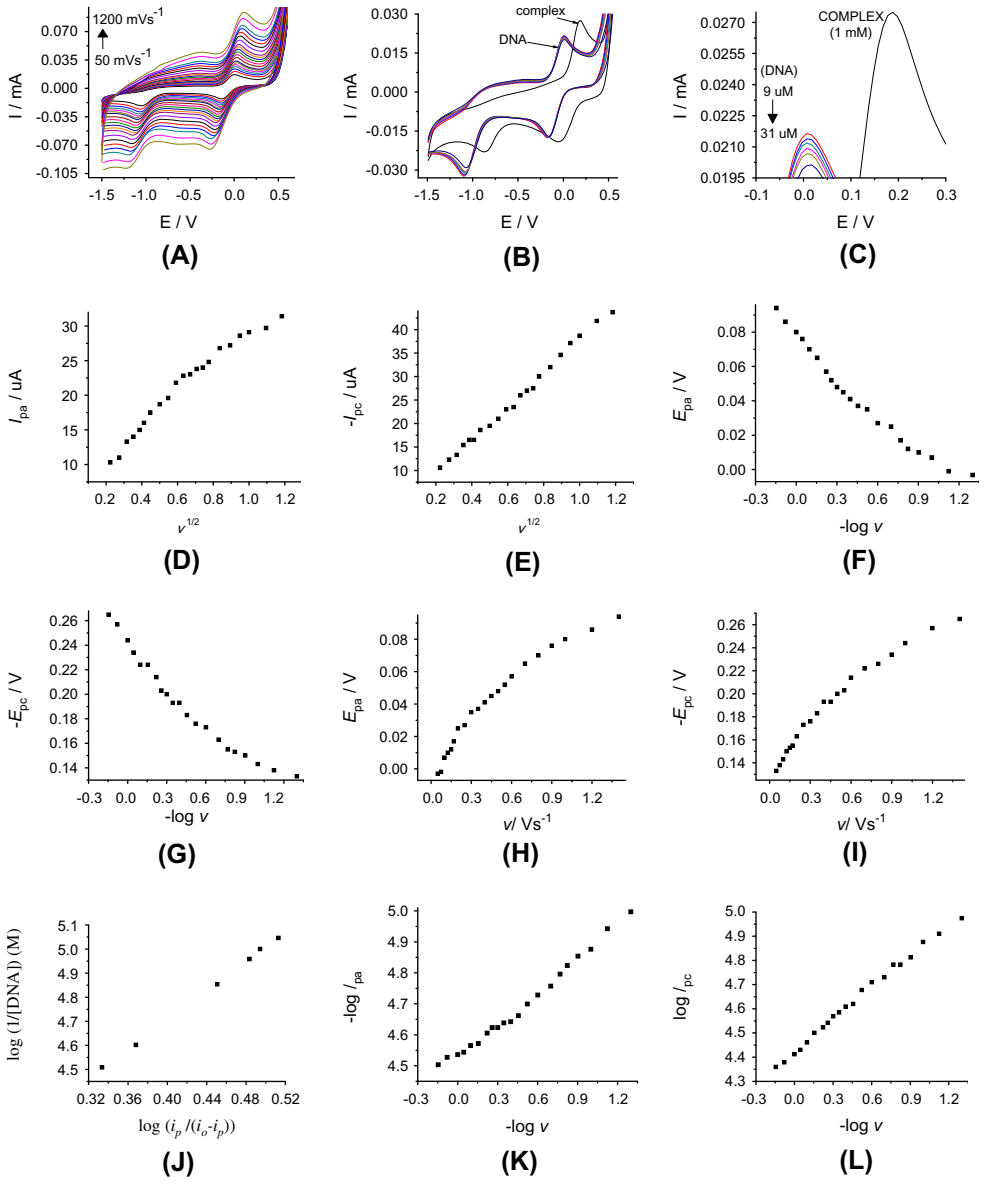

Figure 8. (A) Current *vs.* potential plots at scan rates of 50, 75, 100, 125, 150, 175, 200, 250, 300, 350, 400, 450, 500, 550, 600, 700, 800, 900, 1000, and 1200 mV s^{-1} of the complex (1 mM) in the presence of 25 µM DNA; (B) current *vs.* potential plots of pure complex and in the presence of 9, 10, 11, 14, 25, and 31 µM DNA at 100 mV s^{-1} in full potential window (–1.5 to 0.5 V); (C) oxidation peaks of plot B; plots D–L (data taken from plot A); (D) i_{pa} *vs.* $v^{1/2}$; (E) $-i_{pc}$ *vs.* $v^{1/2}$; (F) E_{pa} *vs.* $-\log v$; (G) $-E_{pc}$ *vs.* $-\log v$; (H) E_{pa} *vs.* v; (I) $-E_{pc}$ *vs.* v; (J) log (1/[DNA]) *vs.* log (i_p/i_o-i_p); (K) $-\log i_{pa}$ *vs.* $-\log v$ (slope = 0.349); (L) log i_{pc} *vs.* $-\log v$ (slope = 0.440).

3.6. *DNA study through absorption spectroscopy*

The absorption spectrum of the complex in the absence and presence of SSDNA is shown in figure 9(A) with a band at 720 nm, corresponding to the d–d transition of Cu^{2+}. On

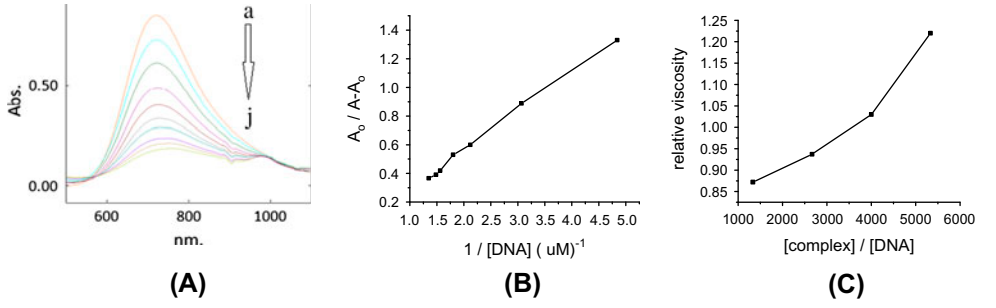

Figure 9. (A) Absorption spectra of 4 mM complex in the absence (a) and presence of 0.0375 (b), 0.075 (c), 0.112 (d), 0.150 (e), 0.187 (f), 0.225 (g), 0.262 (h), 0.281 (i) and 0.300 μM DNA (j). The arrow direction indicates the increasing concentration of SSDNA. (B) Plot of $A_o/(A - A_o)$ *vs.* 1/[DNA] for the determination of binding constant of complex-SSDNA adduct. (C) Effect of increasing amount of the complex on the relative viscosity of SSDNA at 25 ± 0.1 °C where [DNA] = 7.5×10^{-8} M.

successive addition of SSDNA, there is a bathochromic shift indicating intercalation with the complex. By making use of Benesi–Hildebrand equation [67], the binding constant, calculated based upon the variation in absorbance, was 1.436×10^3 M^{-1} [plot shown in figure 9(B)]. The value of the binding constant matches well with that calculated through cyclic voltammetry.

3.7. *Viscosity measurements*

In order to further clarify the binding mode of complex with SSDNA, viscosity measurements were carried out. As evident from figure 9(C), there is a marked increase in the relative viscosity of SSDNA with successive addition of the complex, indicating a classical intercalation mode of interaction with SSDNA helix.

4. Conclusion

Dimeric Cu(II) complex of N and O donors has been synthesized and characterized. X-ray crystal structure exhibited Cu(II) in square-pyramidal geometry. Powder XRD confirms the purity of the complexes. The relatively larger potential difference between Cu(III)/Cu(II) and Cu(II)/Cu(I) redox couples of the complex has been attributed to the relatively stable Cu(II) species under the experimental conditions. Predominantly diffusion-controlled electron transfer processes were indicated by the slope values of $-\log i_p$ *versus* $-\log v$ plots. Interesting DNA-binding activity has been observed for the complex as indicated by the significant change in various voltammetric variables such as D_o and $k°$ of the complex, calculated before and after DNA addition. Cyclic voltammetry exhibited a mixed electrostatic as well as intercalative mode of interaction for the complex with SSDNA, with a binding constant value of 3.074×10^3 M^{-1}. The DNA-binding ability of the complex was confirmed from UV–visible spectrophotometry as well as viscometry, both of which indicated an intercalative mode of interaction for the complex, with a binding constant value of 1.436×10^3 M^{-1}. The complex follows both electrostatic and intercalative modes of interaction with SSDNA. The complex

Downloaded by [Institute Of Atmospheric Physics] at 15:14 09 December 2014

exhibited facile metal-based electron transfer processes and DNA-binding ability which can find applications in many research areas.

Supplementary material

Crystallographic data for the structure of the complex reported in this article has been deposited with the Cambridge Crystallographic Data Center, CCDC # 899281. Copy of the information may be obtained free of charge from The Director, CCDC, 12 Union Road, Cambridge CB2 1EZ [Fax: +44 1223 336 033 or Email: deposit@ccdc.cam.ac.uk].

Downloaded by [Institute Of Atmospheric Physics] at 15:14 09 December 2014

Acknowledgment

M. Iqbal is thankful to the Higher Education Commission of Pakistan for providing scholarship under Indigenous Ph.D. Fellowship Program as well as International Research Support Initiative Program (IRSIP) and the authors are thankful for the crystal structure analysis performed on the Australian synchrotron.

References

[1] A. Prisecaru, M. Devereux, N. Barron, M. McCann, J. Colleran, A. Casey, V. McKee, A. Kellett. *Chem. Commun.*, **48**, 6906 (2012).
[2] R.E. Windsor, S.J. Strauss, C. Kallis, N.E. Wood, J.S. Whelan. *Cancer*, **118**, 1856 (2012).
[3] J.T. Wang, Q. Xia, X.H. Zheng, H.Y. Chen, H. Chao, Z.W. Mao, L.N. Jia. *Dalton Trans.*, 2128 (2010).
[4] C.H. Ng, K.C. Kong, S.T. Von, P. Balraj, P. Jensen, E. Thirthagiri, H. Hamada, M. Chikira. *Dalton Trans.*, 447 (2008).
[5] J.B. Tommasino, G. Pilet, F.N.R. Renaud, G. Novitchi, V. Robert, D. Luneau. *Polyhedron*, **37**, 27 (2012).
[6] E. Reisner, V.B. Arion, B.K. Keppler, A.J.L. Pombeiro. *Inorg. Chim. Acta*, **361**, 1569 (2008).
[7] C.S. Cano, M.J. Hannon. *Dalton Trans.*, 10702 (2009).
[8] T.W. Hambley. *Science*, **318**, 1392 (2007).
[9] P.C.A. Bruijnincx, P.J. Sadler. *Curr. Opin. Chem. Biol.*, **12**, 197 (2008).
[10] N. Graf, S.J. Lippard. *Adv. Drug Deliv. Rev.*, **64**, 993 (2012).
[11] T.W. Hambley. *Dalton Trans.*, 4929 (2007).
[12] W.R. Wilson, M.P. Hay. *Nat. Rev. Cancer*, **11**, 393 (2011).
[13] B.A. Teicher. *Cancer Metastasis Rev.*, **13**, 139 (1994).
[14] Y. Chen, L. Hu. *Med. Res. Rev.*, **29**, 29 (2009).
[15] J.M. Brown, A.J. Giaccia. *Cancer Res.*, **58**, 1408 (1998).
[16] M.H. Torre, D. Gambino, J. Araujo, H. Cerecetto, B. González, M.L. Lavaggi, A. Azqueta, A.L. de Cerain, A.M. Vega, U. Abram, A.J. Costa-Filho. *Eur. J. Med. Chem.*, **40**, 473 (2005).
[17] C. Urquiola, D. Gambino, M. Cabrera, M.L. Lavaggi, H. Cerecetto, M. González, A.L. de Cerain, A. Monge, A.J. Costa-Filho, M.H. Torre. *J. Inorg. Biochem.*, **102**, 119 (2008).
[18] P.J. Blower, J.R. Dilworth, R.I. Maurer, G.D. Mullen, C.A. Reynolds, Y. Zheng. *J. Inorg. Biochem.*, **85**, 15 (2001).
[19] B.G. Bharate, A.N. Jadhav, S.S. Chavan. *Polyhedron*, **33**, 179 (2012).
[20] S.S. Massoud, L.L. Quan, K. Gatterer, J.H. Albering, R.C. Fischer, F.A. Mautner. *Polyhedron*, **31**, 601 (2012).
[21] C.W. Yeh, K.H. Chang, C.Y. Hu, W. Hsu, J.D. Chen. *Polyhedron*, **31**, 657 (2012).
[22] I. Gracia-Mora, L. Ruiz-Ramírez, C. Gómez-Ruiz, M. Tinoco-Méndez, A. Márquez-Quiñones, L. Romero-De Lira, A. Marín-Hernández, L. Macías-Rosales, M.E. Bravo-Gómez. *Met. Base. Drugs*, **8**, 19 (2001).
[23] R.A. De Vizcaya, M.A. Rivero, R.L. Ruiz, G.E.N. Kass, L.R. Kelland, R.M. Orr, M. Dobrota. *Toxicol. In Vitro*, **14**, 1 (2000).
[24] C. Mejia, L.R. Azuara. *Pathol. Oncol. Res.*, **14**, 467 (2008).
[25] S. Fountoulaki, F. Perdih, I. Turel, D.P. Kessissoglou, G. Psomas. *J. Inorg. Biochem.*, **105**, 1645 (2011).
[26] C. Tolia, A.N. Papadopoulos, C.P. Raptopoulou, V. Psycharis, C. Garino, L. Salassa, G. Psomas. *J. Inorg. Biochem.*, **123**, 53 (2013).

[27] D. Panagoulis, E. Pontiki, E. Skeva, C. Raptopoulou, S. Girousi, D. Hadjipavlou-Litina, C. Dendrinou-Samara. *J. Inorg. Biochem.*, **101**, 623 (2007).
[28] W.-H. Wang, W.-S. Liu, Y.-W. Wang, Y. Li, L.-F. Zheng, D.-Q. Wang. *J. Inorg. Biochem.*, **101**, 297 (2007).
[29] T.M. McPhillips, S.E. McPhillips, H.J. Chiu, A.E. Cohen, A.M. Deacon, P.J. Ellis, E. Garman, A. Gonzalez, N.K. Sauter, R.P. Phizackerley, S.M. Soltis, P. Kuhn. *J. Synchrotron Radiat.*, **9**, 401 (2002).
[30] W. Kabsch. *Acta Cryst.*, **D 66**, 125 (2010).
[31] G.M. Sheldrick. *Acta Cryst.*, **A 64**, 112 (2008).
[32] S. Dey, S. Sarkar, H. Paul, E. Zangrando, P. Chattopadhyay. *Polyhedron*, **29**, 1583 (2010).
[33] C.V. Sastri, D. Eswaramoorthy, L. Giribabu, B.G. Maiya. *J. Inorg. Biochem.*, **94**, 138 (2003).
[34] S. Mathur, S. Tabassum. *Cent. Eur. J. Chem.*, **4**, 502 (2006).
[35] G. Eng, X. Song, A. Zapata, A.C. de Dios, L. Casabiana, R.D. Pike. *J. Organomet. Chem.*, **692**, 1398 (2007).
[36] G.B. Deacon, R.J. Phillips. *Coord. Chem. Rev.*, **33**, 227 (1980).
[37] C.G. Mohamed, Z.H. Abd El-Wahab. *J. Therm. Anal. Calorim.*, **73**, 347 (2003).
[38] C. Jayabalakrishnan, K. Natarajan. *Transition Met. Chem.*, **27**, 75 (2002).
[39] Z.H. Abd El-Wahab, M.M. Mashaly, A.A. Salman, B.A. El-Shetary, A.A. Faheim. *Spectrochim. Acta, Part A*, **60**, 2861 (2004).
[40] L.Y. Wang, Q.Y. Chen, J. Huang, K. Wang, C.J. Feng, Z.R. Gen. *Transition Met. Chem.*, **34**, 337 (2009).
[41] I. Fomina, Z. Dobrokhotova, G. Aleksandrov, A. Bogomyakov, M. Fedin, A. Dolganov, T. Magdesieva, V. Novotortsev, I. Eremenko. *Polyhedron*, **29**, 1734 (2010).
[42] I.G. Fomina, Z.V. Dobrokhotova, G.G. Aleksandrov, M.A. Kiskin, M.A. Bikov, V.N. Ikorskii, V.M. Novotortsev, I.L. Eremenko. *Russ. Chem. Bull.*, **56**, 1722 (2007).
[43] A. Motreff, R.C. Costa, H. Allouchi, M. Duttine, C. Mathoniere, C. Duboc, J.M. Vincent. *J. Fluorine Chem.*, **134**, 49 (2012).
[44] E.M. Rustoy, M. Agotegaray, O.E. Piro, E.E. Castellano. *J. Coord. Chem.*, **65**, 2341 (2012).
[45] Y.-M. Li, C.-Y. Xiao, H.-R. Feng, S.-S. Guo, S.-B. Wang. *J. Coord. Chem.*, **65**, 2820 (2012).
[46] P.M. Selvakumar, S. Nadella, J. Sahoo, E. Suresh, P.S. Subramanian. *J. Coord. Chem.*, **66**, 287 (2013).
[47] J. Zhou, L. Du, Z. Li, Y. Qiao, J. Liu, M. Zhu, P. Chen, Q. Zhao. *J. Coord. Chem.*, **66**, 2166 (2013).
[48] M. Iqbal, I. Ahmad, S. Ali, N. Muhammad, S. Ahmed, M. Sohail. *Polyhedron*, **50**, 524 (2013).
[49] A.H. Pathan, R.P. Bakale, G.N. Naik, C.S. Frampton, K.B. Gudasi. *Polyhedron*, **34**, 149 (2012).
[50] J.P. Naskar, B. Guhathakurta, L. Lu, M. Zhu. *Polyhedron*, **43**, 89 (2012).
[51] M.A. Neelakantan, F. Rusalraj, J. Dharmaraja, S. Johnsonraja, T. Jeyakumar, M.S. Pillai. *Spectrochim. Acta, Part A*, **71**, 1599 (2008).
[52] K. Abdi, H. Hadadzadeh, M. Weil, M. Salimi. *Polyhedron*, **31**, 638 (2012).
[53] S. Timári, R. Cerea, K. Várnagy. *J. Inorg. Biochem.*, **105**, 1009 (2011).
[54] S. Majumder, M. Fleck, C.R. Lucas, S. Mohanta. *J. Mol. Struct.*, **1020**, 127 (2012).
[55] S. Meghdadi, K. Mereiter, V. Langer, A. Amiri, R.S. Erami, A.A. Massoud, M. Amirnasr. *Inorg. Chim. Acta*, **385**, 31 (2012).
[56] I. Ucar, B. Karabulut, A. Bulut, O. Buyukgungor. *J. Mol. Struct.*, **834–836**, 336 (2007).
[57] H.A. Alghamdi, F.F. Belal, M.A. Al-Omar. *J. Pharm. Biomed. Anal.*, **41**, 989 (2006).
[58] J. Wang. *Analytical Electrochemistry*, 1st Edn, pp. 165–166, VCH Publishers, Weinheim (1994).
[59] A.J. Bard, L.R. Faulkner. *Electrochemical Methods, Fundamentals and Applications*, 2nd Edn, p. 236, Wiley, New York, NY (2004).
[60] E. Laviron. *J. Electroanal. Chem.*, **52**, 335 (1974).
[61] E. Laviron. *J. Electroanal. Chem.*, **101**, 19 (1979).
[62] A.J. Bard, L.R. Faulkner. *Electrochemical Methods, Fundamentals and Applications*, 2nd Edn, p. 552, Wiley, New York, NY (1980).
[63] M.T. Carter, M. Rodriguez, A.J. Bard. *J. Am. Chem. Soc.*, **111**, 8901 (1989).
[64] Q.X. Wang, F. Gao, K. Jiao. *Electroanalysis*, **20**, 2096 (2008).
[65] M. Chauhan, K. Banerjee, F. Arjmand. *Inorg. Chem.*, **46**, 3072 (2007).
[66] Q. Feng, N.Q. Li, Y.Y. Jiang. *Anal. Chim. Acta*, **344**, 97 (1997).
[67] S. Shujha, A. Shah, Z. Rehman, N. Muhammad, S. Ali, R. Qureshi, N. Khalid, A. Meetsma. *Eur. J. Med. Chem.*, **45**, 2902 (2010).

Downloaded by [Institute Of Atmospheric Physics] at 15:14 09 December 2014